TRENDS IN SCIENCES 2026; 23(3): 11684
https://doi.org/10.48048/tis.2026.11684 RESEARCH ARTICLE

Harnessing Metal-Loaded Zeolites for Superior Antibacterial Activity

Sriatun[1,*], Tania[1], Siti Nursyamsiah[1], Adi Darmawan[1], Choiril Azmiyawati[1], Damar Nurwahyu Bima[1] and Nor Aida Zubir[2]

[1]Department of Chemistry, Faculty of Science and Mathematics, Diponegoro University, Semarang 50275, Indonesia
[2]Chemical Engineering Studies, College of Engineering, Universiti Teknologi MARA, Cawangan Pulau Pinang, Permatang Pauh 13500, Malaysia

([*]Corresponding author's e-mail: sriatun@live.undip.ac.id)

Received: 25 August 2025, Revised: 2 October 2025, Accepted: 12 October 2025, Published: 15 December 2025

Abstract

Metal-loaded zeolites has gained significant interest for their antibacterial properties and potential applications in biomedical and environmental fields. In this study, silver- and copper-loaded zeolites were successfully synthesized using ion exchange and impregnation methods. Characterization techniques confirmed the successful incorporation of Ag^{+} and Cu^{2+} ions into the zeolite framework. X-ray diffraction (XRD) analysis demonstrated reduction in peak intensities at $2\theta \approx 26°$, 34° and 42° for Ag-zeolite and $2\theta = 19.59°$, 32.22° and 37.97° for Cu-zeolite, indicating successful metal loading. Scanning Electron Microscopy-Energy Dispersive X-ray Spectroscopy (SEM-EDX) verified the presence of 3.98% Ag and 3.79% Cu in the modified zeolites. The antibacterial performance of Ag- and Cu-loaded zeolites was evaluated against *Escherichia coli* and *Staphylococcus aureus* using disk diffusion and well diffusion methods. Ag-zeolite (0.05 M, 9 h) exhibited inhibition zones of 12.23 mm and 11.35 mm for *E. coli* and *S. aureus*, respectively. Cu-zeolite showed even stronger antibacterial activity, with inhibition zones of 15.3 mm and 18.1 mm. These findings highlight the potential of Ag- and Cu-loaded zeolites as effective antimicrobial agents. This research demonstrates a simple and efficient approach for synthesizing antibacterial zeolites, offering promising applications in water treatment, wound healing and antibacterial coatings. This research can serve as a reference for further studies, including the evaluation of long-term stability and the exploration of practical applications for large-scale implementation.

Keywords: Zeolite, Antibacterial activity, Metal ion loading, *Escherichia coli*, *Staphylococcus aureus*

Introduction

Antibacterial materials have emerged as advanced materials, particularly in field of health, tropical diseases, nutrition and pharmaceuticals. The increasing prevalence of bacterial infections has necessitated the development of effective antibacterial agents. Traditionally, antibiotics have been widely used as antibacterial agents, aiding the immune system in halting bacterial infections. However, prolonged and improper use of antibiotics have led to the emergence of antibiotic-resistant bacteria, posing a serious global health concern [1]. This highlights the urgent need for the development of safer and environmentally friendly antibacterial materials.

Recent advancements have focused on the utilization of reliable and cost-effective antibacterial agents, particularly modified zeolite-based materials [2]. As an inorganic material, zeolite offers unique advantages as an antibacterial carrier due to its heat resistance, high chemical stability, prolonged durability, and safety for users [3]. The high cation-exchange capacity of zeolites, resulting from their large surface area and negatively charged framework, makes them suitable carriers for metal ions with antibacterial properties [4].

The antibacterial performance of zeolite can be significantly enhanced by modification with metal ions. Metals such as silver (Ag), copper (Cu) and zinc (Zn)

exhibit potent antimicrobial properties [5]. Silver ions (Ag^+), for instance, possess broad-spectrum antibacterial activity with low toxicity in humans. They disrupt bacterial proteins and cell membranes by interacting with disulfide (S–S) and sulfhydryl (–SH) groups, forming S–Ag bonds that lead to bacterial inactivation and cell death [6]. Copper ions (Cu^{2+}) can disturb membrane integrity, while zinc ions (Zn^{2+}) have been widely employed to inhibit cariogenic bacteria in dental applications [7].

Previous studies have demonstrated the potential of modified zeolites as antibacterial agents. For instance, Yao *et al*. [8] found that Cu-Zeolite X exhibited superior antibacterial activity against *Escherichia coli* and *Staphylococcus aureus*, while Milenkovic *et al*. [9] reported that Ag-Zeolite A showed the highest inhibition against *Escherichia coli* when compared to Cu- and Zn-modified zeolites. Furthermore, Ishak *et al*. [10] revealed the efficacy of silver-modified kaolinite zeolite in inhibiting the growth of both Gram-positive and Gram-negative bacteria. Lastly, Mintcheva, *et al*. [11] in his study investigates how exchangeable ions in natural and modified zeolites influence silver (Ag) content, Ag nanoparticles (AgNPs) formation, and their antibacterial effectiveness. The modified zeolites served as carriers for Ag ions, which were later reduced to form AgNPs within the zeolite structure. The study found that the type of exchangeable ion significantly affected the distribution and stability of AgNPs, influencing their antibacterial activity.

However, despite these promising findings, several critical gaps remain in the current literature. Few studies have provided a comprehensive analysis of the long-term stability of metal-loaded zeolites or their antibacterial performance under diverse environmental conditions and against multiple bacterial strains. Additionally, the environmental impact of their use, including potential metal ion leaching and toxicity, has not been thoroughly explored. Comparative analyses of modified zeolites with other antibacterial agents in terms of efficacy, cost-effectiveness and scalability are also limited. Moreover, challenges related to scaling up the synthesis process for industrial applications, including reproducibility, consistency and economic feasibility, have rarely been addressed [12].

From all this previous study, its sugested that zeolite, especially when modified with metal ions such as Ag, Cu and Zn, is an effective antibacterial material. The exchangeable ions in zeolites play a crucial role in determining their silver content, Ag nanoparticle (AgNP) formation and overall antibacterial performance. Ag-modified zeolites exhibit the highest antibacterial efficacy, particularly against *Escherichia coli* and *Staphylococcus aureus*, due to their ability to release Ag^+ ions and form stable AgNPs within the zeolite structure [13]. Additionally, different metal modifications, such as Cu and Zn, also contribute to antibacterial activity, although their effectiveness varies depending on the zeolite type and ion-exchange process [14]. These findings highlight the potential of modified zeolites as promising antibacterial agents for various applications, but also underscore the need for further studies addressing stability, environmental impact, and scalability.

Given these promising results, this study aims to synthesize zeolites with a low Si/Al ratio through various synthesis methods and subsequently modify them with Ag^+ and Cu^{2+} ions. The antibacterial performance of the modified zeolites will be evaluated against *Escherichia coli* and *Staphylococcus aureus*. This research not only seeks to develop highly efficient, stable and sustainable antibacterial materials but also aims to provide insights that could inform long-term applications and industrial-scale implementation.

Experimentals

Materials

The materials used in this study include sodium aluminate (Sigma-Aldrich), sodium silicate (Merck; density 1.35 g/cm³), SiO_2/LUDOX HS-40 (Sigma-Aldrich; colloidal silica), sodium hydroxide (NaOH, 98% purity, Merck; anhydrous pellets), ethanol (70% purity, Merck), deionized water, silver nitrate ($AgNO_3$, 99.0 - 99.97% purity, Merck), copper(II) nitrate trihydrate ($Cu(NO_3)_2 \cdot 3H_2O$, Merck), zinc nitrate hexahydrate ($Zn(NO_3)_2 \cdot 6H_2O$, Sigma-Aldrich), Whatman No.42 filter paper (Whatman), universal pH indicator strips (pH range 0–14, Merck), nutrient agar (Technical grade, Merck), nutrient broth (Technical grade, Merck), test microbes (*Escherichia coli ATCC 25922*, *Staphylococcus aureus ATCC 25923*) and chloramphenicol (Technical grade, Merck).

Synthesis of zeolite

A total of 17.45 g of NaOH was dissolved in deionized water to prepare 266.17 mL of 1.69 M NaOH solution. Subsequently, 16.4 g of sodium aluminate ($NaAl_2O$) was added to the NaOH solution, resulting in a 0.75 M $NaAl_2O$ solution. Next, 277.103 mL of the 0.75 M $NaAl_2O$ solution was mixed with 11.6 mL of LUDOX. The mixture was stirred using magnetic stirrer at moderate speed and room temperature until it became homogeneous and slightly viscous.

The resulting mixture was transferred into a closed Teflon vessel and heated in a microwave at medium power for 1 h. Afterward, the mixture was aged at room temperature for 24 h. The solid product was filtered and washed with deionized water until neutral pH was achieved. The solid was then dried at 80 °C until a constant weight was obtained, yielding synthetic zeolite.

For the combined microwave-hydrothermal method, the same composition was used. The mixture was heated in a microwave at medium power for 5 min, followed by hydrothermal treatment at 150 °C for 24 h

Metal loading onto zeolite

Variation in Ag^+ Ion loading concentration

A total of 1 g of synthetic zeolite was mixed with 10 mL of $AgNO_3$ solution at varying concentrations (0.03, 0.04, 0.05, 0.06, 0.07 M) and stirred for 5 h. The product was filtered, washed and dried at 80 °C for 3 h to obtain Ag^+-loaded zeolite (M).

Variation in Ag^+ Ion loading time

A total of 1 g of synthetic zeolite was mixed with 10 mL of 0.05 M $AgNO_3$ solution and stirred using a magnetic stirrer for different durations (3, 6, 9, 12, 24 h). The product was filtered, washed and dried at 80 °C for 3 h to produce Ag^+-loaded zeolite (t).

Variation in Cu^{2+} Ion loading concentration

The metal loading method on synthetic zeolite was adapted from Septommy *et al*. [15]. A total of 1 g of synthetic zeolite was mixed with 10 mL of $Cu(NO_3)_2 \cdot 3H_2O$ solution at varying concentrations (0.03, 0.04, 0.05, 0.06, 0.07 M) and stirred for 9 h. The product was filtered, washed and dried at 80 °C for 3 h to obtain Cu^{2+}-loaded zeolite (M).

Variation in Cu^{2+} Ion loading time

A total of 1 g of synthetic zeolite was mixed with 10 mL of 0.05 M $Cu(NO_3)_2 \cdot 3H_2O$ solution and stirred using a magnetic stirrer at 400 rpm for different durations (3, 6, 9, 12, 24 h). The product was filtered, washed and dried at 80 °C for 3 h to produce Cu^{2+}-loaded zeolite (t).

Characterization

All synthesized products were characterized for their crystallinity and phase using X-ray diffraction (XRD), functional groups using Fourier-transform infrared spectroscopy (FTIR) and surface morphology as well as elemental composition using scanning electron microscopy with energy-dispersive X-ray spectroscopy (SEM-EDX). The zeolite loaded with metal ions was further characterized using XRD and SEM-EDX.

Antibacterial activity test of metal ion-loaded zeolites

Preparation of mcfarland standard solution

A total of 0.05 mL of 1% $BaCl_2$ was mixed with 9.95 mL of H_2SO_4 and stored away from direct sunlight. The absorbance value was then measured at a wavelength of 600 nm.

Preparation of Nutrient Agar (NA) media

A total of 2.3 g of NA powder was dissolved in 100 mL of distilled water, stirred, and heated on a hot plate. The solution was autoclaved at 121°C and 1.5 atm for 15 min. Subsequently, 10 mL of the medium was poured into sterile petri dishes.

Preparation of Nutrient Broth (NB) media

A total of 0.8 g of NB powder was dissolved in 100 mL of distilled water, stirred, and heated on a hot plate. The solution was autoclaved at 121 °C and 1.5 atm for 15 min. Subsequently, 10 mL of the medium was poured into sterile petri dishes.

Rejuvenation of S. aureus and E. coli bacteria

S. aureus or *E. coli* colonies were taken from bacterial stock on slanted agar medium using an inoculation loop and inoculated into an Erlenmeyer flask aseptically near a Bunsen burner in a laminar air flow (LAF). The culture was incubated in a shaker incubator

at 37 °C for 24 h to obtain *S. aureus* or *E. coli* colonies.
2.6 Preparation of *S. aureus* and *E. coli* Bacterial Suspensions.

S. aureus or *E. coli* bacteria were inoculated into NB media aseptically near a Bunsen burner in a laminar air flow (LAF). The culture was incubated in a shaker incubator at 37 °C and absorbance at 600 - 625 nm was measured every 2 - 3 h until the absorbance matched that of the McFarland 0.5 standard solution, corresponding to a bacterial count of 1.5×10^8 CFU/mL.

Antibacterial test with *S. aureus* and *E. coli*

Well diffusion method

A total of 0.1 mL of *S. aureus* or *E. coli* bacterial suspension was spread evenly on NA agar medium using a spreader. Five wells with a diameter of 6 mm were created in the agar medium. Each well was filled with 30 mg of metal ion-loaded zeolite dissolved in 50 µL of distilled water. The plates were incubated at 37 °C for 24 h and the diameter of the inhibition zones was measured using a ruler. The average diameter of the inhibition zones was recorded. The same procedure was applied to positive control (Chloramphenicol), negative control (distilled water) and sample control ($AgNO_3$, $Cu(NO_3)_2$ and $Zn(NO_3)_2$) using *S. aureus* and *E. coli*.

Disk diffusion method

The antibacterial test using the disk diffusion method was performed with Whatman No. 42 filter paper as the disk material. The agar medium, which had been inoculated with 0.1 mL of *S. aureus* or *E. coli* bacterial suspension, was overlaid with filter paper disks soaked in the sample solution. The plates were incubated at 37 °C for 24 h and the diameter of the inhibition zones was measured using a caliper. The average diameter of the inhibition zones was recorded. The same procedure was applied to positive control (Chloramphenicol), negative control (distilled water) and sample control ($AgNO_3$, $Cu(NO_3)_2$ and $Zn(NO_3)_2$) using *S. aureus* and *E. coli*.

Results and discussion

Characteristics of synthesized zeolite

The X-ray diffraction (XRD) analysis of the synthesized zeolite with a low molar ratio (Si/Al = 1) revealed the formation of Zeolite X, as evidenced by specific diffraction peaks at 2θ values of 10.31°, 24.13°, 26.30°, 27.26°, 30.09°, 30.94°, 32.66°, 34.32° and 42.77° as shown in **Figure 1(a)**. These peaks were compared with the reference patterns from the JCPDS database and previous studies [16,17], which confirmed that the synthesized zeolite was predominantly Zeolite X, with a mixture ratio of 55.61% Zeolite X and 44.39% Zeolite A. This composition was determined using the Search and Match software, which matched the observed diffraction peaks to those of Zeolite X and A standards.

Because of its high ion exchange capacity due to the abundance of balancing cations, low molar ratio of Si/Al ~ 1 is chosen. Low Si/Al ratio zeolites (1 - 5) are typically classified as faujasite (FAU) structures with large pores (~7.4 Å) [18]. This zeolite used Na^+ as the balancing cation which originated from the excess NaOH during synthesis that facilitates the dissolution of silica and alumina and accelerates crystallization process. Silica and alumina tetrahedral units underwent polymerization to form a negatively charged silica-alumina framework stabilized by Na^+ [19]. Homogenized mixtures of $NaAl_2O$ and LUDOX gradually thickened and turned white at room temperature, indicating the formation of zeolite precursors. $NaAl_2O$ served as the alumina source, while LUDOX provided silica. Microwave heating followed by 24 h of aging stabilized the formation of synthetic zeolite crystals.

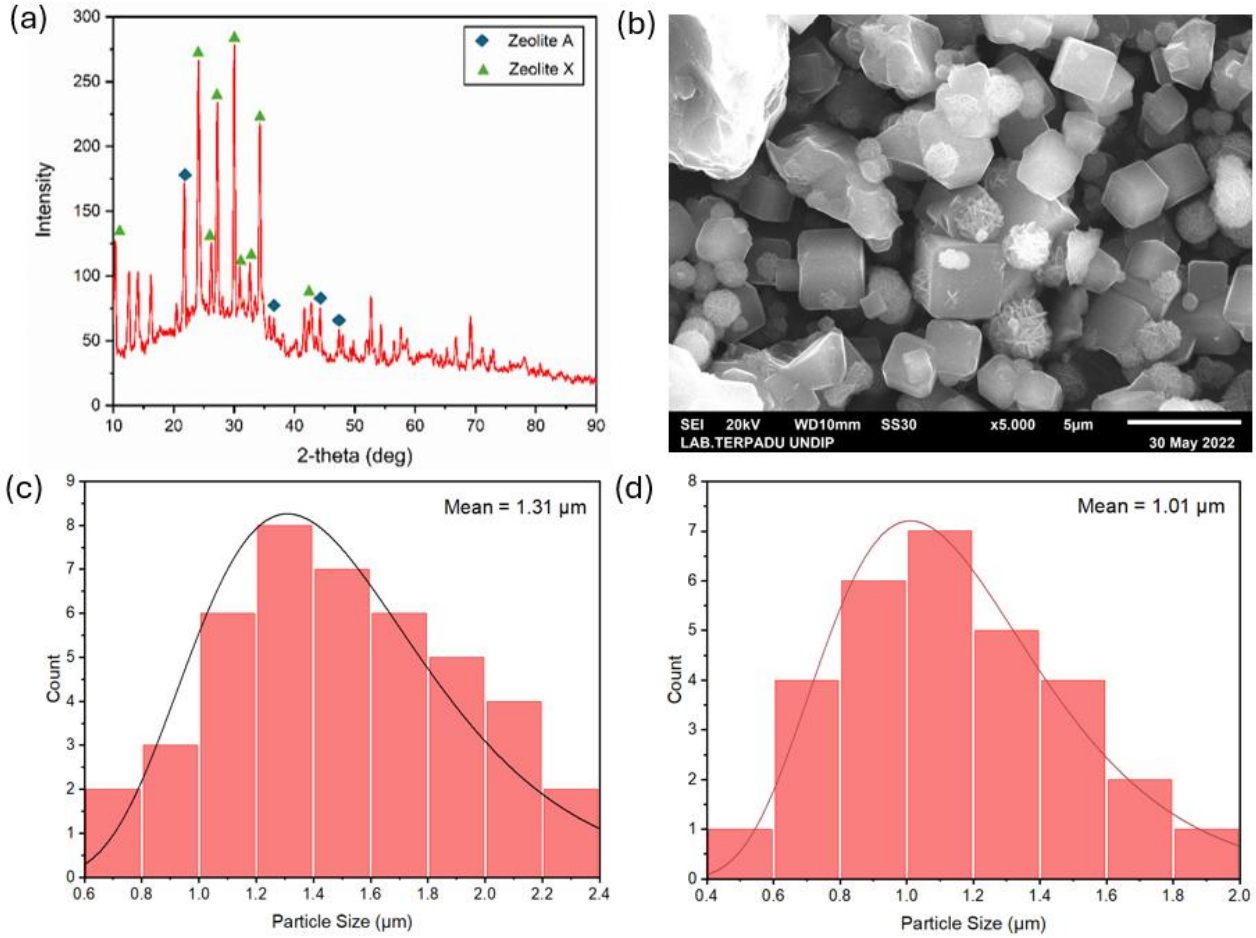

Figure 1 (a) XRD diffractogram of the synthesized zeolite, confirming the presence of Zeolite A (♦) and Zeolite X (▲) based on characteristic peaks. (b) SEM image showing the morphology of the synthesized zeolite particles in magnification 5,000×. Particle size distribution of (c) Zeolite A and (d) Zeolite X. Particle size measurements were obtained from the SEM image using ImageJ software.

The SEM image (**Figure 1(b)**) showed the morphology of the synthesized zeolite particles, revealing the characteristic crystal structures of Zeolite A and Zeolite X. Zeolite A exhibited a cubic morphology, whereas Zeolite X showed spherical to polyhedral particles. The well-defined crystal shapes indicated successful zeolite crystallization without significant amorphous phases [20].

The particle size distributions of Zeolite A and Zeolite X were analysed using ImageJ software (**Figures 1(c) - 1(d)**). Zeolite A particles have an average size of 1.31 µm, with a relatively broad distribution ranging from 0.6 to 2.4 µm. In contrast, Zeolite X particles obtained slightly smaller size with an average of 1.01 µm and exhibited a narrower size distribution (0.4 - 2.0 µm). The differences in particle size and morphology can be attributed to the synthesis conditions, particularly nucleation rate, growth time and NaOH concentration, which influence the crystallization pathways of different zeolite phases [21].

Characteristics of metal-modified zeolites

Crystall properties of metal-modified zeolites

The modification of zeolites with metal ions, such as silver (Ag^{+}) and copper (Cu^{2+}), enhances their functional properties, including antimicrobial activity and catalytic performance. Understanding the structural stability and ion-exchange behavior of metal-loaded zeolites is crucial for optimizing their applications [22]. In this study, X-ray diffraction (XRD) analysis was conducted to investigate the structural effects of silver and copper ion exchange on the synthesized zeolite.

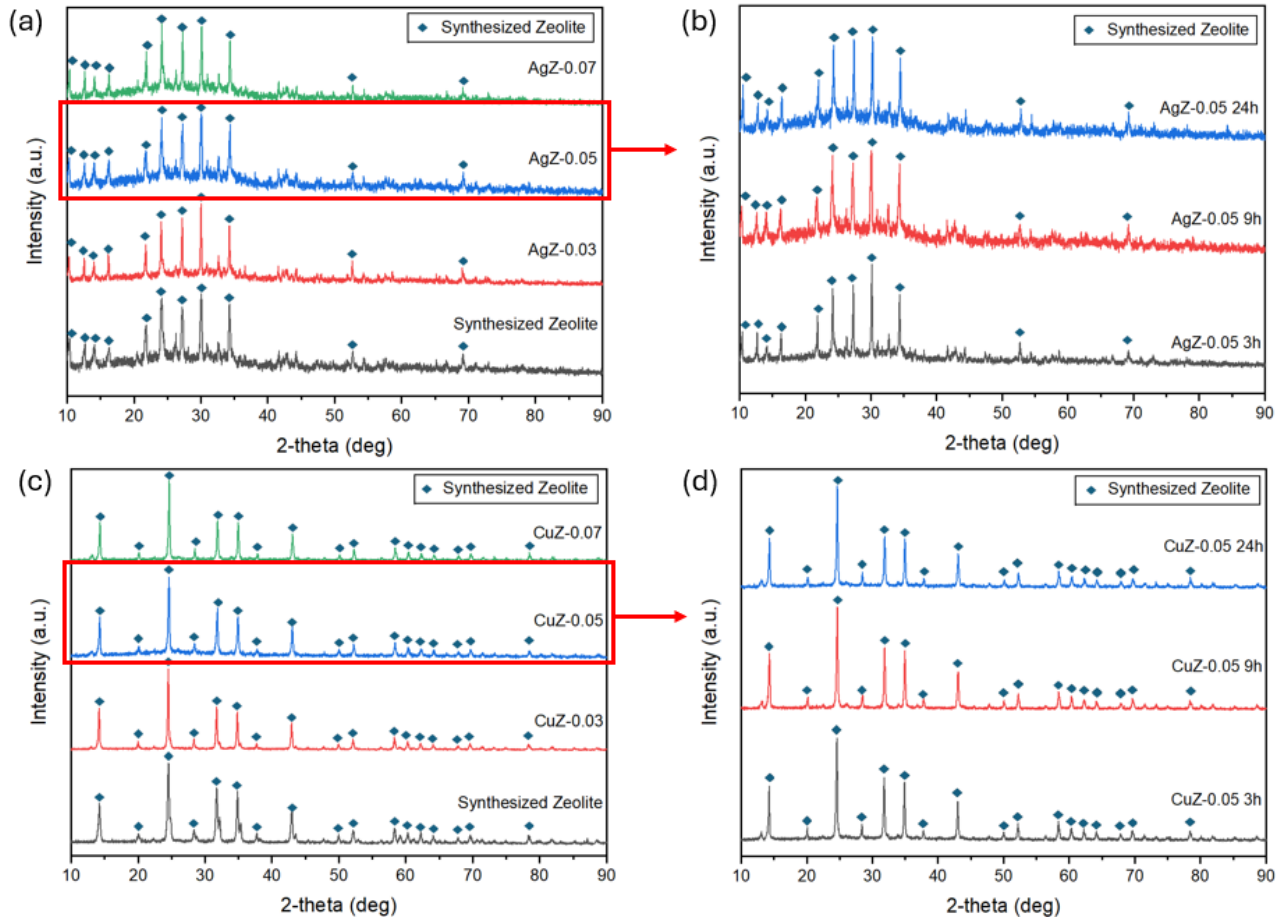

Figure 2 (a) XRD patterns of the synthesized zeolite and silver-modified zeolite (AgZ) at different silver ion concentrations (0.03 M, 0.05 M and 0.07 M) with a fixed loading time of 9 h. (b) XRD patterns of AgZ with 0.05 M silver ion loading at different durations (3, 9 and 24 h). (c) XRD patterns of the synthesized zeolite and copper-modified zeolite (CuZ) at different copper ion concentrations (0.03 M, 0.05 M and 0.07 M) for 9 h. (d) XRD patterns of CuZ with 0.05 M copper ion loading at different loading time (3, 9 and 24 h).

The effect of silver ion modification on the zeolite structure was analyzed by loading silver ions with different concentrations (0.03 M, 0.05 M and 0.07 M) for varying times (3, 9 and 24 h). The XRD analysis, shown in **Figures 2(a) - 2(b)**, indicated that despite the introduction of silver ions, no significant changes in the diffraction peaks occurred. This suggests that the overall crystalline structure of zeolite was well-preserved [23]. However, a notable decrease in the intensity of the diffraction peaks was observed, which indicates the ion exchange between sodium (Na^+) ions in the zeolite framework with silver (Ag^+) ions [24]. The most pronounced decrease in intensity was seen at 2θ values of ~26°, 34° and 42°, confirming successful silver incorporation [25]. The reduced peak intensities were attributed to a slight distortion in the zeolite lattice due to the difference in ionic radii between Ag^+ and Na^+, as well as the potential formation of Ag nanoparticles within the zeolite pores at higher silver concentrations.

Similarly, the XRD patterns of copper-modified zeolite in **Figures 2(c) - 2(d)** exhibited a reduction in diffraction peak intensities, particularly at 19.59°, 32.22° and 37.97° that indicate the successful incorporation of copper ions. The average crystallite size of the synthesized zeolite was calculated to be 35.67 nm using the Full Width at Half Maximum (FWHM) parameter [26]. Upon exchanging with copper ions, the decrease in peak intensity suggests partial substitution of Na^+ with Cu^{2+}, leading to minor structural modifications. Peak intensity decreased progressively with increasing ion-exchange duration, particularly at 24 h, implying a time-dependent effect on metal loading [27]. However, no new diffraction peaks corresponding to copper oxides or metallic copper were detected,

confirming that Cu^{2+} remained in the ion-exchanged state within the zeolite framework. The relatively low intensity of Cu-loaded zeolite peaks suggests that the amount of incorporated copper was limited, potentially due to competition between ion exchange and adsorption onto external sites of the zeolite particles.

Surface morphology of metal-modified zeolites

The surface morphology and elemental composition of the silver-modified and copper-modified zeolite samples were analyzed using Scanning Electron Microscopy (SEM) and Energy Dispersive X-ray (EDX).

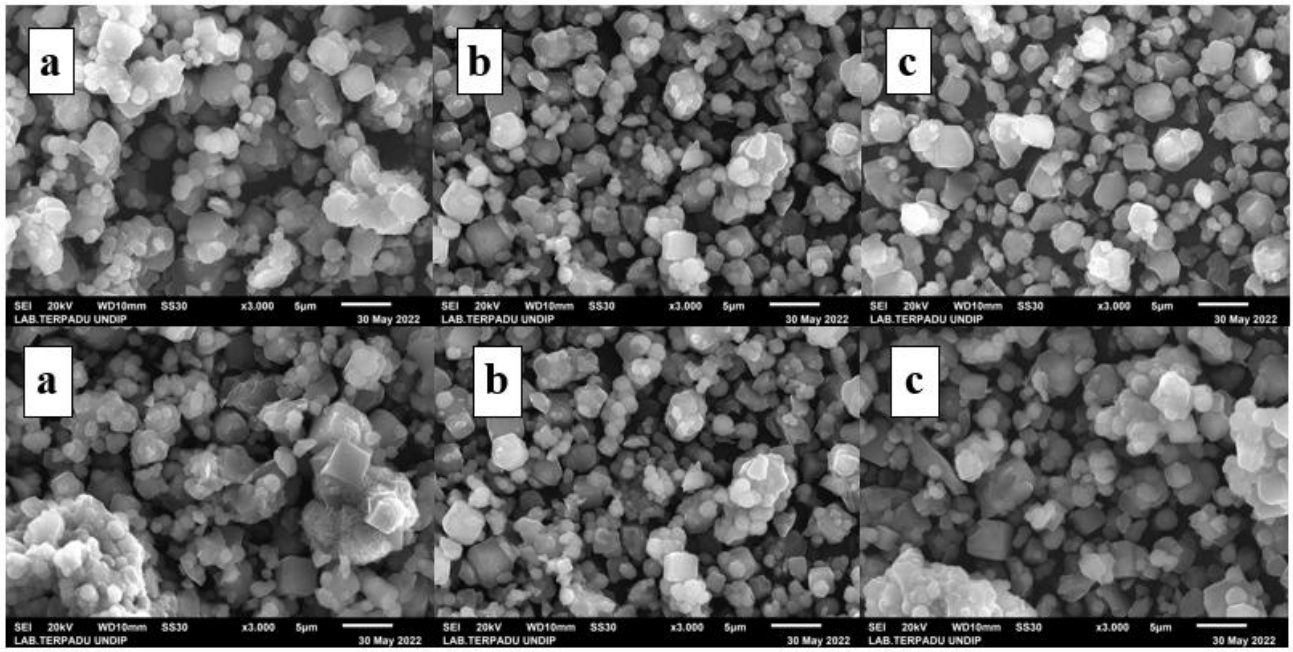

Figure 3 (1) Ag^+-loaded zeolite at concentrations of (a) 0.03 M, (b) 0.05 M and (c) 0.07 M after 9 h of ion loading and (2) Ag^+-loaded zeolite a (a) 3 h, (b) 9 h and (c) 24 h on 0,05 M.

For the Ag-zeolite samples, modifications were performed with varying silver nitrate concentrations (0.03 M, 0.05 M, 0.07 M) and different loading times (3, 9 and 24 h) (**Figure 3**). The SEM images revealed uniform morphology, with crystal shapes corresponding to Zeolite X and Zeolite A, specifically octahedral and cubic forms, which is consistent with previous studies [28]. Upon modification with silver ions, the SEM micrographs showed that Ag^+ ions were well-dispersed on the zeolite surface and the crystals formed aggregates with varying sizes [29,30]. However, the presence of larger aggregates suggested some agglomeration due to the ion exchange process. The EDX analysis revealed in **Table 1** that the synthesized zeolite contained Si, Al, Na, O and Ag. The molar ratio of Si/Al in the unmodified zeolite was found to be relatively low (1.11 to 1.16). When modified with silver ions, a decrease in sodium content was observed, indicating that Na^+ ions were exchanged with Ag^+ ions during the modification process. The sample modified with 0.07 M $AgNO_3$ showed a higher Ag^+ content but also a relatively high Na^+ content, indicating incomplete ion exchange, where silver ions may still be bound to the zeolite surface.

Table 1 Elemental analysis results using EDX on synthesized zeolite and synthesized Ag-zeolite.

Sample	Elemental Distribution (% mass)					Mol Ratio Si/Al
	Si	Al	Na	O	Ag	
Synthesized Zeolite	8.84	9.88	9.47	53.58	-	1.16
AgZ-1	10.63	11.38	10.67	54.01	1.92	1.11
AgZ-2	7.99	8.82	8.31	51.8	1.98	1.14
AgZ-3	8.8	9.6	8.1	50.71	4.58	1.13
AgZ-2 3h	10.07	10.8	9.24	50.22	3.98	1.11
AgZ-2 9h	6.33	6.74	6.59	49.16	2.18	1.10

For the Cu-zeolite samples in **Figure 4**, similar modifications were carried out, with varying copper ion concentrations (0.03 M, 0.05 M, 0.07 M) and different loading times (3, 9 and 24 h). SEM analysis of the Cu-zeolite samples revealed no significant changes in morphology compared to the unmodified zeolite, with small octahedral-shaped particles forming aggregates. The EDX results on synthesized zeolite in **Table 2** confirmed that copper ions had successfully exchanged with Na^+ ions in the zeolite structure, as evidenced by the decrease in sodium content and the incorporation of copper. The Si/Al molar ratio for the Cu-zeolite samples ranged from 0.88 to 0.95, indicating the ion exchange was successful [31]. However, the sample modified with 0.07 M $CuSO_4$ showed the highest copper content, suggesting that a higher concentration of copper led to more copper ions being loaded onto the zeolite. Despite this, the sodium content remained somewhat high, indicating that the ion exchange was not fully completed and some sodium ions were still strongly bound within the zeolite structure.

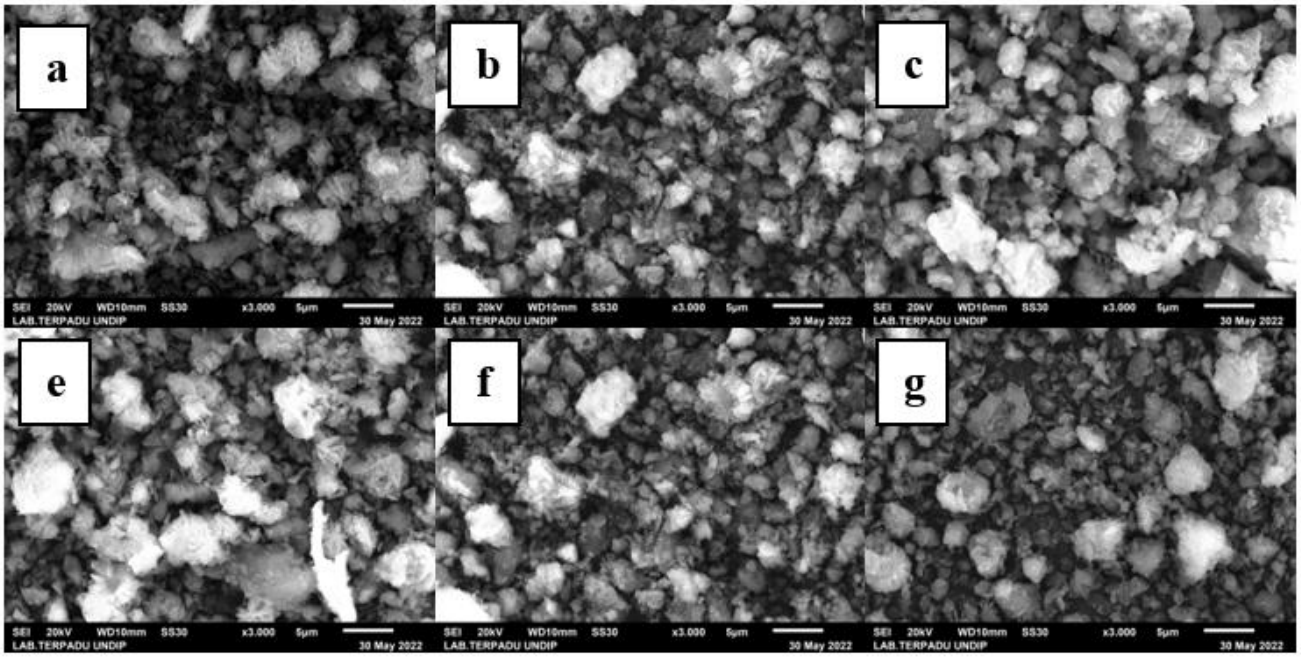

Figure 4 Morphology of Cu-zeolite samples: (a) Cu-Z 0.03 M, (b) Cu-Z 0.05 M, (c) Cu-Z 0.07 M, (d) Cu-Z 3 H, (e) Cu-Z 9 H and (f) Cu-Z 24 H.

In both cases, the ion exchange processes were influenced by the concentration of metal ions and the duration of loading. While silver and copper ions were successfully incorporated into the zeolite, some incomplete ion exchange and surface adsorption of metal ions were observed, which could impact their further applications [32].

Table 2 Elemental analysis results using EDX on synthesized zeolite and synthesized Cu-zeolite.

Sample	Elemental Distribution (% Mass)					Si/Al Ratio
	Si	Al	Na	O	Cu	
Synthesized Zeolite	11.39	12.27	12.3	64.04	-	0.93
CuZ-1	11.42	12.41	11.43	61.96	2.78	0.92
CuZ-2	8.26	9.43	8.57	70.94	2.81	0.88
CuZ-3	12.89	13.59	9.49	58.51	5.51	0.95
CuZ-2 3h	10.96	12.16	10.00	63.09	3.79	0.90
CuZ-2 9h	8.26	9.43	8.57	70.94	2.81	0.88
CuZ-2 24h	7.12	7.87	7.81	74.40	2.80	0.90

Antibacterial activity of metal-modified zeoliyes

The antibacterial activity of metal-loaded zeolites was evaluated using both the disc diffusion and well diffusion methods against *Escherichia coli* (Gram-negative) and *Staphylococcus aureus* (Gram-positive). Silver- and copper-loaded zeolites were synthesized by ion exchange with varying concentrations of $AgNO_3$ and $Cu(NO_3)_2$ and the inhibition zones were measured to assess antibacterial efficacy. The results of this antibacterial activity is shown in **Figure 5**.

The results demonstrate that increasing silver nitrate ($AgNO_3$) concentration and loading time enhanced antibacterial activity. In the disc diffusion method, the largest inhibition zones were observed at a 0.05 M $AgNO_3$ concentration, with values of 12.23 mm for *E. coli* and 11.35 mm for *S. Aureus* as shown in **Figures 5(a) - 5(b)**. While, in the well diffusion method, the inhibition zones reach up to 13.32 mm for *E. coli* and 13.24 mm for *S. aureus*. On the other hand, copper-loaded zeolite exhibited stronger antibacterial properties, with the best performance observed at a 0.05 M $Cu(NO_3)_2$ concentration, similar to the silver-loaded sample, where inhibition zones reached 15.3 mm (*E. coli*) and 18.1 mm (*S. aureus*) in the disc diffusion method. In the well diffusion method, the inhibition zones were even larger, at 19.3 mm and 22.6 mm, respectively. When comparing the two methods, the well diffusion assay produced larger inhibition zones than the disc diffusion method, suggesting that metal ions diffuse more effectively when directly incorporated into the agar medium. In contrast, the disc diffusion method may have limited ion mobility due to the fixed amount of metal-loaded zeolite in the disc.

Both silver- and copper-loaded zeolites exhibited optimal antimicrobial performance at a precursor concentration of 0.05 M. Although antimicrobial activity generally increases with higher metal loading, a decline in efficacy was observed when the concentration exceeded this threshold. This reduction can be attributed to pore blockage by excess metal ions at elevated concentrations, which decreases the material's effective surface area. This interpretation is consistent with the study of Fanta, *et al*. [33], who reported that the adsorption capacity of copper-doped zeolite increased with loading in the range of 0.63 - 6.3 g, but declined at higher amounts, as evidenced by reduced iodine values that indicate fewer accessible active sites. Our EDX analysis further supports this explanation: At precursor concentrations above 0.05 M, the spectra revealed substantially higher metal contents within the zeolite structure, confirming that additional ions were incorporated beyond the optimal level. Such excessive loading likely results in partial pore clogging and a

reduction in exchangeable sites, thereby limiting ion release and decreasing the overall antimicrobial activity. Since surface area and ion availability are both critical for bacterial contact and inhibition, the combination of restricted diffusion and diminished active sites explains the observed plateau or decline in antibacterial performance despite higher metal incorporation.

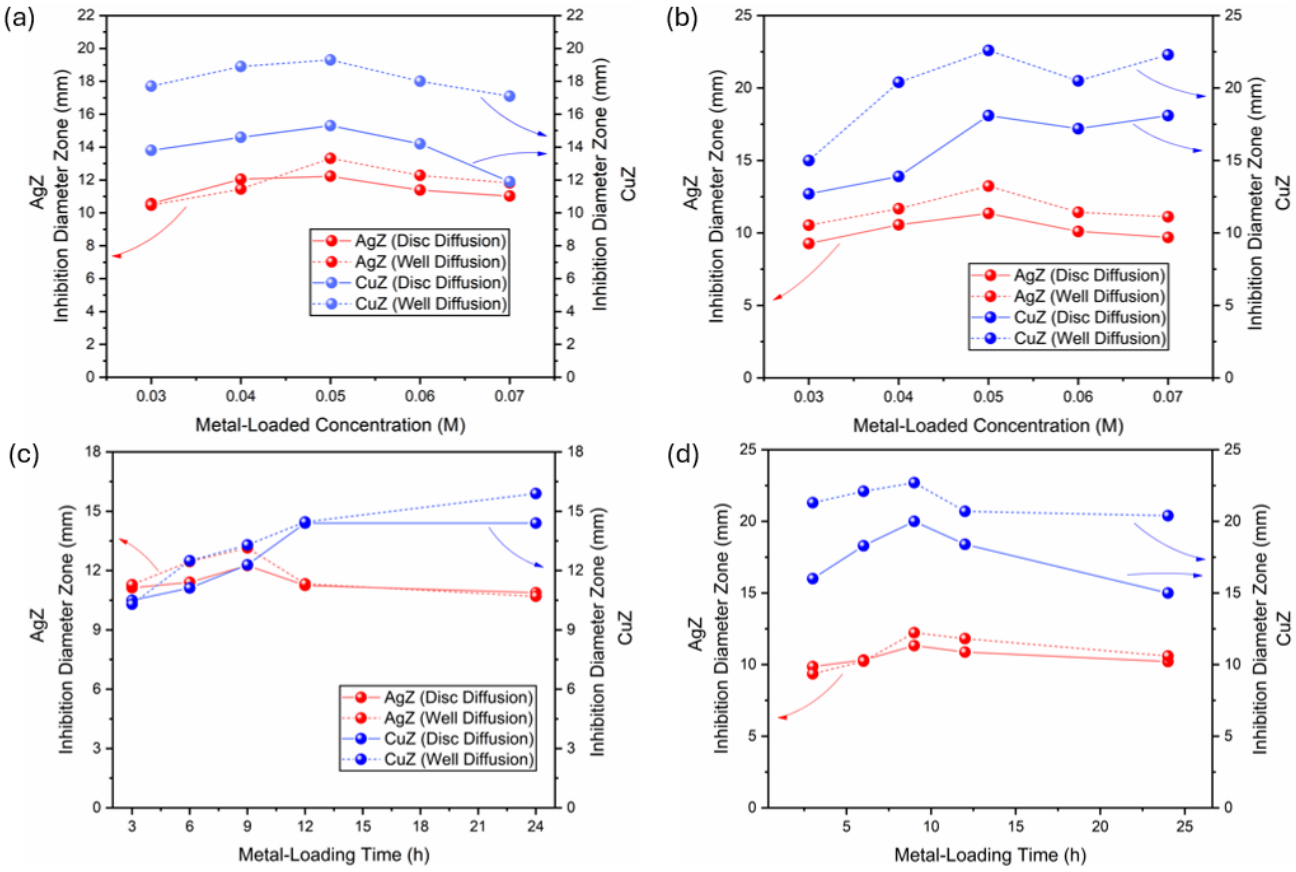

Figure 5 (a) Inhibition zone diameters for *E. coli* at varying metal-loaded concentrations. (b) Inhibition zone diameters for *S. aureus* at varying metal-loaded concentrations. (c) Inhibition zone diameters for *E. coli* at different metal-loading times. (d) Inhibition zone diameters for *S. aureus* at different metal-loading times. The antibacterial activity was assessed using disc diffusion and well diffusion methods. Chloramphenicol was used as the positive control, while distilled water served as the negative control.

The time-dependent study of silver- and copper-loaded zeolites revealed that the optimal loading time for antibacterial activity was 9 h. At this condition, silver-loaded zeolite exhibited inhibition zones of 12.26 mm against *E. coli* and 11.33 mm against *S. aureus* in the disc diffusion method (**Figures 5(b) - 5(c)**). A comparable trend was observed in the well diffusion assay, with inhibition zones of 13.15 mm and 12.23 mm, respectively. In contrast, copper-loaded zeolite achieved inhibition zones of 14.6 mm (*E. coli*) and 18.1 mm (*S. aureus*) in the disc diffusion method, while the well diffusion method yielded even larger zones, measuring 20.5 mm and 22.6 mm, respectively. Longer loading times beyond 9 h showed diminishing returns. This phenomenon may be attributed to the saturation of the zeolite structure, which reduces the release rate of Ag^{+} and Cu^{2+} ions. Prolonged loading increases the amount of metal ions within the pores, thereby limiting their subsequent release into solution or agar. The fraction of leachable metal further decreases, due to stronger ion–framework interactions or the full occupation of exchangeable sites.

Silver and Copper ions exhibit antibacterial activity through two primary mechanisms: (1) disruption of bacterial membranes via electrostatic interactions, leading to leakage of intracellular contents

and (2) generation of reactive oxygen species (ROS), which cause oxidative damage to DNA and protein [34]. Compared to silver, copper displayed stronger antibacterial effects, particularly against *S. aureus*. This effect may be attributed to the smaller ionic radius of Cu^{2+} (73 pm) compared to Ag^{+} (116 pm). The reduced size facilitates more efficient penetration through outer membrane porin channels, thereby enhancing bactericidal activity relative to Ag^{+} [35]. In addition, the electrochemical properties of Ag^{+} contribute to its lower stability in biological environments. With a standard reduction potential of +0.80 V (Ag^{+}/Ag), Ag^{+} is more readily reduced to metallic silver under physiological conditions [36]. This reduction decreases the concentration of bioavailable ions capable of interacting with bacterial cells, ultimately limiting its antimicrobial performance. By contrast, Cu^{2+} possesses a lower reduction potential, allowing it to remain in its ionic form for longer periods and sustain ion release, thereby maintaining stronger antimicrobial efficacy.

The study highlights distinct antibacterial profiles for silver- and copper-loaded zeolites. While both metals showed strong antibacterial effects, copper demonstrated superior inhibition zones, particularly against *S. aureus*. This difference can be attributed to structural features of Gram-positive cell envelopes. Unlike Gram-negative bacteria, which possess a thin peptidoglycan layer (~8 nm), Gram-positive bacteria have a much thicker peptidoglycan matrix (20 - 80 nm) enriched with anionic wall teichoic acids (WTAs) [37]. These glycopolymers, composed of polyribitol or polyglycerol phosphates, carry a high density of negatively charged phosphate groups that readily bind divalent cations [38]. Such binding sites act as reservoirs for metal ions and play a key role in charge neutralization and cell wall stability. Consequently, Cu^{2+} ions exhibit strong electrostatic affinity toward these anionic sites, particularly phosphate and carboxylate groups, leading to enhanced accumulation and interaction with the Gram-positive cell wall. This preferential binding likely contributes to the greater antibacterial efficacy of copper against *S. aureus*.

Although Ag^{+} exhibited lower overall antibacterial activity compared to Cu^{2+}, it showed stronger inhibition against *E. coli* (Gram-negative) than *S. aureus* (Gram-positive). This selectivity can be explained by differences in cell wall structure. Gram-negative bacteria possess a relatively thin peptidoglycan layer, which allows Ag^{+} ions, despite their larger ionic radius, to diffuse more readily through the cell envelope. In contrast, Gram-positive bacteria have a much thicker peptidoglycan matrix, which acts as a stronger physical barrier and limits Ag^{+} penetration. As a result, silver-loaded zeolite demonstrates greater antibacterial efficacy against *E. coli* than *S. aureus*.

Both materials show potential for use in antibacterial coatings, water treatment, and medical applications. Silver-loaded zeolite may be preferable in scenarios requiring controlled ion release, whereas copper-loaded zeolite is more effective for applications requiring strong antibacterial action, particularly against Gram-positive bacteria. The findings provide valuable insights for optimizing metal-modified zeolites for specific antibacterial applications based on bacterial strain and required ion release kinetics.

Conclusions

In this study, silver- and copper-loaded zeolite materials were successfully synthesized using ion exchange and impregnation methods, as described in the methodology. Characterization results confirmed the successful incorporation of metal ions into the zeolite framework. XRD analysis revealed a pronounced decrease in peak intensity at $2\theta = 26°$, 34°, and 42° for Ag-zeolite, confirming silver incorporation. Similarly, Cu-zeolite exhibited a reduction in diffraction peak intensities at $2\theta = 19.59°$, 32.22° and 37.97°, indicating the successful integration of copper ions. SEM images demonstrated uniform particle distribution with minimal aggregation, while EDX analysis verified the elemental composition, indicating 3.98% Ag and 3.79% Cu in the modified zeolites. Antibacterial testing revealed that both Ag-zeolite and Cu-zeolite exhibited significant inhibition against *E. coli* and *S. aureus*. In the disk diffusion method, Ag-zeolite (0.05 M, 9 h) produced inhibition zones of 12.23 mm for *E. coli* and 11.35 mm for *S. aureus*, while Cu-zeolite (0.05 M, 9 h) achieved inhibition zones of 15.3 mm and 18.1 mm, respectively. The well diffusion method showed even larger inhibition zones. These results demonstrate the potential of metal-loaded zeolites as effective antibacterial materials for biomedical and environmental applications. Future work will focus on optimizing

synthesis conditions and assessing long-term stability in real-world applications.

Acknowledgment

The authors gratefully acknowledge the financial support provided by the Dean of the Faculty of Science and Mathematics, Diponegoro University for funding this research under contract No. 21/UN7.F8/PP/II/2023.

Credit Authorship Contribution

Sriatun: Conceptualization; Funding acquisition; Project administration; Resources; Supervision; Validation; Writing – review & editing. **Tania**: Data curation; Formal analysis; Methodology; Writing – original draft. **Siti Nursyamsiah**: Data curation; Methodology; Investigation; Writing – original draft. **Adi Darmawan**: Supervision; Validation; Conceptualization; Writing – review & editing. **Choiril Azmiyawati**: Supervision; Validation; Visualization; Writing – original draft. **Damar Nurwahyu Bima**: Supervision; Validation; Writing – review & editing. **Nor Aida Zubir**: Resources; Validation; Writing – review & editing.

References

[1] L Serwecińska. Antimicrobials and antibiotic-resistant bacteria: A risk to the environment and to public health. *Water* 2020; **12(12)**, 3313.

[2] Y Verma, G Sharma, A Kumar, T Wang, P Dhiman and GT Mola. Zeolites and their composites as novel remediation agent for antibiotics: A review. *Environmental Engineering Research: EER* 2025; **30(1)**, 240062.

[3] J Matusiak, A Przekora and W Franus. Zeolites and zeolite imidazolate frameworks on a quest to obtain the ideal biomaterial for biomedical applications: A review. *Materials Today* 2023; **67**, 495-517.

[4] S Dabagh, SA Haris, BK Isfahani, N Ashammakhi and YN Ertas. Zeolite-copper ferrite nanocomposites with improved antibacterial activity and reusability for biomedical applications. *ACS Applied Nano Materials* 2023; **6(22)**, 21412-21423.

[5] X Fan, LH Yahia and E Sacher. Antimicrobial properties of the Ag, Cu nanoparticle system. *Biology* 2021; **10(2)**, 137.

[6] M Awais, A Aizaz, A Nazneen, QA Bhatti, M Akhtar, A Wadood and MAU Rehman. A review on the recent advancements on therapeutic effects of ions in the physiological environments. *Prosthesis* 2022; **4(2)**, 263-316.

[7] X Ma, S Zhou, X Xu and Q Du. Copper-containing nanoparticles: Mechanism of antimicrobial effect and application in dentistry-a narrative review. *Frontiers in Surgery* 2022; **9**, 905892.

[8] G Yao, J Lei, W Zhang, C Yu, Z Sun, S Zheng and S Komarneni. Antimicrobial activity of X zeolite exchanged with Cu(2+) and Zn(2+) on escherichia coli and staphylococcus aureus. *Environmental Science and Pollution Research International* 2019; **26(3)**, 2782-2793.

[9] J Milenkovic, J Hrenovic, D Matijasevic, M Niksic and N Rajic. Bactericidal activity of Cu-, Zn- and Ag-containing zeolites toward escherichia coli isolates. *Environmental Science and Pollution Research International* 2017; **24(25)**, 20273-20281.

[10] S Ishak, NANN Malek, Z Yusop, CD Williams, S Suhartono and A Syafiuddin. Evaluation of phase transformation behaviors of zeolite and antibacterial properties against Gram-positive and -negative bacteria. *Journal of the Chinese Chemical Society* 2020; **67(11)**, 2042-2049.

[11] N Mintcheva, M Panayotova, G Gicheva, O Gemishev and G Tyuliev. Effect of exchangeable ions in natural and modified zeolites on Ag content, Ag nanoparticle formation and their antibacterial activity. *Materials* 2021; **14(15)**, 4153.

[12] J Hrenović and N Rajić. Application of modified natural zeolite—clinoptilolite for bacterial control in the environment. *Materials* 2025; **18(10)**, 2411.

[13] X Yang, Q Yu, W Gao, X Tang, H Yi and X Tang. The mechanism of metal-based antibacterial materials and the progress of food packaging applications: A review. *Ceramics International* 2022; **48(23A)**, 34148-34168.

[14] P Peixoto, JF Guedes, E Rombi, AM Fonseca, CA Aguiar and IC Neves. Metal Ion–Zeolite materials against resistant bacteria, MRSA. *Industrial & Engineering Chemistry Research* 2021; **60(35)**, 12883-12892.

[15] C Septommy, SA Nikmatus and B Muarofah. The effect of natural Zeolite (Ag-Zeolite) modified with silver against the inhibition of Candida albicans. *Journal of Syiah Kuala Dentistry Society* 2020; **5(2)**, 56-60.

[16] A Ali, YW Chiang and RM Santos. X-ray diffraction techniques for mineral characterization: A review for engineers of the fundamentals, applications, and research directions. *Minerals* 2022; **12(2)**, 205.

[17] SH Vreeswijk and BM Weckhuysen. Emerging analytical methods to characterize zeolite-based materials. *National Science Review* 2022; **9(9)**, nwac047.

[18] C Koop-Santa, RI Yocupicio-Gaxiola, FN Murrieta-Rico, M Avalos-Borja, M Xiao, V Petranovskii and A Reyes-Serrato. Additive-free synthesis of layer-like Faujasite-type zeolite X. *Journal of Materials Science* 2024; **59**, 10169-10181.

[19] D Liang, Y Liu, R Zhang, Q Xie and L Zhang. A review on the influence factors in the synthesis of zeolites and the transformation behavior of silicon and aluminum during the process. *Comments on Inorganic Chemistry* 2024; **44(6)**, 461-497.

[20] CT Chen, K Iyoki, P Hu, H Yamada, K Ohara, S Sukenaga, M Ando, H Shibata, T Okubo and T Wakihara. Reaction kinetics regulated formation of short-range order in an amorphous matrix during zeolite crystallization. *Journal of the American Chemical Society* 2021; **143(29)**, 10986-10997.

[21] N Salahudeen. A review on zeolite: Application, synthesis and effect of synthesis parameters on product properties. *Chemistry Africa* 2022; **5**, 1889-1906.

[22] C Han, J Yang, S Dong, L Ma, Q Dai and J Guo. Zeolite preparation from industrial solid waste: Current status, applications and prospects. *Separation and Purification Technology* 2025; **354(P3)**, 128957.

[23] S Wang, J Vaughan, F Xia, B Etschmann, J Brugger, H Brand and H Peng. Revealing the effect of anions on the formation and transformation of zeolite LTA in caustic solutions: An in situ synchrotron PXRD study. *Crystal Growth & Design* 2023; **23(5)**, 3660-3670.

[24] ÁJ Ruíz-Baltazar, SY Reyes-López, N Méndez-Lozano, NA Medellín-Castillo and R Pérez. Sustainable zeolite–silver nanocomposites via green methods for water contaminant mitigation and modeling approaches. *Nanomaterials* 2024; **14(3)**, 258.

[25] HI Hamoud, F Douma, M Lafjah, F Djafri, O Lebedev, V Valtchev and M El-Roz. Size-dependent photocatalytic activity of silver nanoparticles embedded in ZX-Bi zeolite supports. *ACS Applied Nano Materials* 2022; **5(3)**, 3866-3877.

[26] CQWang, JP Yang, R Huang and YJ Cao. Mechanical activation of natural chalcopyrite for improving heterogeneous Fenton degradation of tetracycline. *Journal of Central South University* 2022; **29**, 3884-3895.

[27] SAF Romeeh, SA Younis, MM Ghobashy, YM Moustafa, MY Abdelaal and MA Deyab. Design a variety of cation exchange hydrogel resins using gamma irradiation to remove hard/scale metal cations from saline water under different circumstances. *Scientific Reports* 2024; **14**, 30512.

[28] S Li, J Li, M Dong, S Fan, T Zhao, J Wang and W Fan. Strategies to control zeolite particle morphology. *Chemical Society Reviews* 2019; **48(3)**, 885-907.

[29] M Liu, Y Ren, J Wu, Y Wang, J Chen, X Lei and X Zhu. Effect of cations on the structure, physico-chemical properties and photocatalytic behaviors of silver-doped zeolite Y. *Microporous and Mesoporous Materials* 2020; **293**, 109800.

[30] S Silviana, GJ Sanyoto and A Darmawan. Preparation of geothermal silica glass coating film through multi-factor optimization. *Jurnal Teknologi (Sciences & Engineering)* 2021; **83(4)**, 41-49.

[31] APMP Alcantara, MLMD Oliveira, JCSD Araújo, RDS Araújo, RKCD Lima, AV Bueno, MEV Silva, PAC Rocha and E Rodríguez-Castellón. Reduction of typical diesel NOx emissions by SCR-NH3 using metal-exchanged natural zeolite and SBA-15 catalysts. *Air* 2023; **1(3)**, 159-174.

[32] A Darmawan, L Karlina, Y Astuti, Sriatun, DK Wang, J Motuzas and JCD Costa. Interlayer free – nickel doped silica membranes for desalination.

IOP Conference Series: Materials Science and Engineering 2017; **172**, 012001.

[33] FT Fanta, AA Dubale, DF Bebizuh and M Atlabachew. Copper doped zeolite composite for antimicrobial activity and heavy metal removal from waste water. *BMC Chemistry* 2019; **13**, 44.

[34] N Mammari, E Lamouroux, A Boudier and RE Duval. Current knowledge on the oxidative-stress-mediated antimicrobial properties of metal-based nanoparticles. *Microorganism* 2022; **10(2)**, 437.

[35] A Javid, M Kumar, S Yoon, JH Lee and JG Han. Size-controlled growth and antibacterial mechanism for Cu:C nanocomposite thin films. *Physical Chemistry Chemical Physics* 2017; **19(1)**, 237-244.

[36] S Agnihotri and NK Dhiman. *Development of Nano-Antimicrobial Biomaterials for Biomedical Applications*. *In*: A. Tripathi and JS Melo (Eds.). Advances in biomaterials for biomedical applications. Springer, Singapore, 2017, p. 479-545.

[37] YN Slavin, J Asnis, UO Häfeli and H Bach. Metal nanoparticles: understanding the mechanisms behind antibacterial activity. *Journal of Nanobiotechnology* 2017; **15**, 65.

[38] KJ Thomas and CV Rice. Equilibrium binding behavior of magnesium to wall teichoic acid. *Biochimica et Biophysica Acta (BBA) - Biomembranes* 2015; **1848(10A)**, 1981-1987.